Element-by-Element Full-Rank Optical Wireless MIMO Systems Using Narrow-Window Angular Filter Designed Based on One-Dimensional Photonic Crystal

Shinya Sugiura, *Senior Member, IEEE*, and Hideo Iizuka, *Member, IEEE*

***Abstract*—In the field of radio-frequency (RF) communications, the multiple-input multiple-output (MIMO) strategy allows us to attain a higher rate of data transfer due to the multipath-rich environment. In contrast, it is challenging to achieve the same rate in a highly correlated channel that is specific to optical wireless communications. In this paper, we propose the novel concept of an element-by-element optical MIMO system that enables the interference-free reception of parallel symbol streams; it achieves this by using an angular filter (AF) with a narrow transparent window. The AF consists of a one-dimensional photonic crystal, and the angular selectivity is obtained by using the extremely small wave vector regime. We demonstrate that the capacity of the proposed system increases linearly with the minimum number of transmit source elements and receive detectors, which is similar to conventional RF MIMO systems.**

***Index Terms*—Angular filter, capacity, MIMO, optical wireless communications, photonic crystal, spatial multiplexing, visible light communications.**

I. Introduction

WHILE light-emitting diodes (LEDs) are energy-efficient devices commonly used to illuminate rooms, they can also be used for wireless signal transmissions; this is known as visible light communications (VLC) [1]–[3]. Since a wide, unlicensed bandwidth is available in the optical regime, VLC is considered a promising complementary approach to future heterogeneous high-speed wireless networks [4]. VLC is typically characterized by a high signal-to-noise ratio (SNR), because it uses a line-of-sight (LOS) channel and uses a limited modulation bandwidth that is specific to white LED devices.

Motivated by the success of high-rate multiple-input multiple-output (MIMO) techniques [5] in radio-frequency (RF) communications, several VLC-MIMO techniques have been developed; these use multiple LED sources at the transmitter and multiple photodetectors at the receiver. One such example, the spatial-multiplexing MIMO technique has been applied to VLC; in this approach, parallel independent symbol streams are transmitted from different transmit LED elements [6]–[11]. The spatial multiplexing enables the transmission rate to increase linearly with the minimum number of transmit and receive elements; it is valid in an ideal uncorrelated-channel scenario that has a full-rank channel matrix. Another approach, the spatial-modulation MIMO technique [12], [13], is also used for VLC [14]–[17], aiming to increase the transmission rate in a manner similar to that of spatial-multiplexing MIMO. Another approach [18], [19] to a VLC-MIMO system aims to attain spatial diversity; it was developed to combat atmospheric turbulence-induced fading in an outdoor free-space optics (FSO) scenario, rather than in an indoor VLC system.

The receiver structures of high-rate spatial-multiplexing VLC-MIMO systems can be classified into two categories: non-imaging [6], [10], [11], [20] and imaging receivers [8], [9]. Non-imaging receivers typically suffer from high correlation in the channel matrix, and hence the spatial-multiplexing VLC-MIMO system exhibits a lower performance than does a simple repetition-coded single-symbol-stream MIMO system [21]. In previous studies of spatial-modulation-based VLC-MIMO systems [17], [21], a power allocation scheme was developed for combating the limitations imposed by a reduced-rank channel matrix; note that this is specific to the VLC-MIMO techniques that use non-imaging receivers. Although this technique may somewhat increase the constrained channel capacity of the spatial-modulation VLC-MIMO, the unconstrained channel capacity remains low. In contrast, the spatial-multiplexing VLC-MIMO assisted by a non-imaging receiver is capable of exploiting an uncorrelated full-rank channel matrix, although it needs precise alignment to ensure that each LED image is received by a dedicated detector, as mentioned in [11].

More recently, in order to combat the limitations imposed by a VLC-specific low-rank MIMO channel matrix, the use of directive receivers has been proposed for spatial-multiplexing VLC-MIMO systems [22]–[25]; in this approach, directive photodetector elements allow the recovery of the rank of the channel matrix. In one approach [22], [24], a prism is positioned on the surface of each photodetector, and this results in a full-rank MIMO channel matrix. The achievable bit error ratio (BER) is obtained by using zero-forcing and minimum-mean-square-error detection algorithms in a channel-uncoded spatial-multiplexing VLC-MIMO scenario, in which a specific modulation scheme is assumed. The effect of the field of view

Manuscript received July 28, 2016; revised September 29, 2013; accepted October 29, 2016. Date of publication October 31, 2016; date of current version November 22, 2016.

S. Sugiura is with the Department of Computer and Information Sciences, Tokyo University of Agriculture and Technology, Tokyo 184-8588, Japan (e-mail: sugiura@ieee.org).

H. Iizuka is with the Toyota Central Research and Development Laboratories, Inc., Nagakute 480-1192, Japan (e-mail: hiizuka@mosk.tytlabs.co.jp).

Color versions of one or more of the figures in this paper are available online at http://ieeexplore.ieee.org.

Digital Object Identifier 10.1109/JLT.2016.2623838

(FOV) on the rank of a MIMO channel matrix has been investigated [23], [25]. It was shown that when the photodetectors have different FOVs, the performance is better, as measured by the BER. In this paper, we consider the use of a non-imaging receiver in the context of high-rate spatial-multiplexing VLC-MIMO systems.[1]

There are various optical components that can be simply implemented into optical systems, and of these, one-dimensional photonic crystals (PCs), which consist of alternating stacks of films made of different materials, provide opportunities for manipulating dispersion diagrams [26]–[28], and this allows the engineering of various wavelength shapes, polarization schemes, and angular responses. Although wavelength and polarization PC filters are commercially available, significant progress has been made in developing angular PC filters [29]–[33]. Recently, a polarization-independent angular transmission PC filter was presented in [34]; this will be our focus.

Against this background, the novel contributions of this paper are as follows. We propose the novel concept of an element-by-element optical MIMO system that enables interchannel-interference- (ICI-) free parallel symbol-stream transmissions over the VLC-specific LOS channels. Specifically, an angular filter (AF) with a narrow window is positioned in front of the photodetector array at the receiver; it is designed to pass element-wise paths between the transmitter and the receiver, and hence the undesired ICI paths are reflected by the AF. Another explicit benefit of our proposed element-by-element VLC-MIMO architecture is that since the multiple streams received at the photodetector array are decoupled without the need to perform any complicated MIMO detection algorithms, the decoding complexity of the parallel streams is significantly lower than that of a conventional spatial-multiplexing receiver. This is especially beneficial when the number of parallel symbol streams is high.

The remainder of this paper is organized as follows. In Section II, we present the model of our proposed parallel VLC-MIMO system that uses a narrow-window AF at the receiver. Then, in Section III, we present the design of a novel photonic-crystal-based AF for the VLC-MIMO. In Section V, we evaluate the performance of our proposed system, and in Section V, we present our conclusions.

II. System Model

A. Basic Architecture

Fig. 1 shows a schematic of the proposed element-by-element spatial-multiplexing VLC-MIMO system that has a narrow-window AF in front of the photodetector array at the non-imaging receiver. The transmitter is installed in the ceiling of the room and is equipped with N_t transmit LEDs, while the receiver has an N_r-element photodetector array. The element spacings at the transmitter and the receiver are d_t and d_r, respectively. In the proposed receiver, a narrow-window AF is situated in front of the photodetector array, and it is used to reduce ICI. The AF is based on the one-dimensional photonic crystal [34]; details of the design are discussed in Section III.

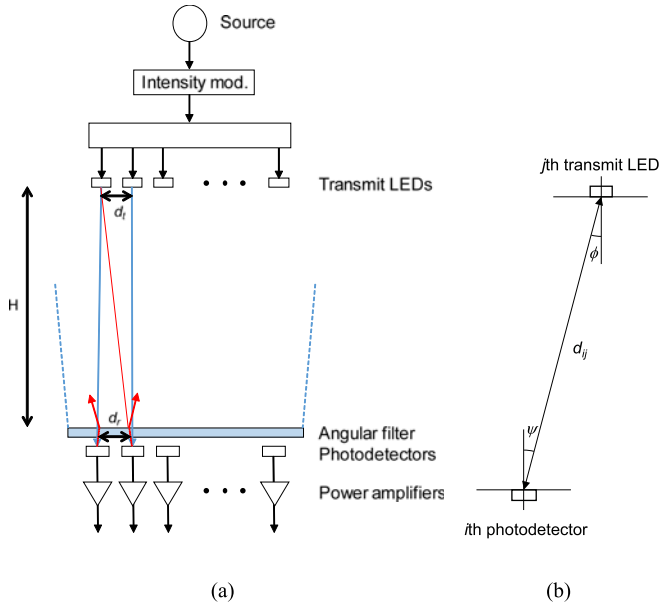

Fig. 1. Schematic of the proposed AF-aided element-by-element MIMO transceiver that has a narrow-window AF in front of the photodetector array at the receiver.

At the transmitter, $B = N_t \log_2 L$ information bits are mapped to real-valued symbols $\mathbf{s} = [s_1, \cdots, s_{N_t}]^T \in \mathbb{R}^{N_t}$, based on intensity modulation of size L, during each symbol interval. The modulated symbols are then serial-to-parallel (S/P) converted and transmitted simultaneously from the N_t transmit LEDs.

Based on previous studies [6], [7], [17], [21], we consider a simplified LOS channel model that is specific to an indoor VLC scenario. Hence, the corresponding received signals $\mathbf{y} = [y_1, \cdots, y_{N_r}]^T \in \mathbb{R}^{N_r}$ are given by

$$\mathbf{y} = \mathbf{H}\mathbf{s} + \mathbf{n}, \tag{1}$$

where $\mathbf{n} = [n_1, \cdots, n_{N_r}]^T \in \mathbb{R}^{N_r}$ are the real-valued additive white Gaussian noise (AWGN) components, which are distributed as $\mathcal{N}(0, \sigma^2)$. The noise variance is the sum of the shot noise variance and the thermal noise variance. Furthermore, $\mathbf{H} \in \mathbb{R}^{N_r \times N_t}$ represents the channel matrix, where the ith-row and the jth-column element h_{ij} corresponds to the channel coefficient between the jth transmit LED and the ith received photo detector; for simplicity, we assume frequency-flat channels.

The channel coefficient h_{ij} is given by [21]

$$h_{ij} = \begin{cases} \dfrac{(k+1)A}{2\pi d_{ij}^2} r(\psi) \cos^k(\phi) \cos(\psi) & 0 \le \psi \le \Psi/2 \\ 0 & \psi \ge \Psi/2 \end{cases}, \tag{2}$$

where

$$k = \frac{-\ln(2)}{\ln(\cos(\Phi/2))}, \tag{3}$$

[1] In general, the detailed fair performance comparison between the imaging and non-imaging VLC receivers is a challenging task, and hence it is left for the future studies.

$\Phi/2$ and $\Psi/2$ are the transmitter semiangle and the receiver's FOV angle, respectively, A is the detection area of each photodetector, and $r(\psi)$ represents the attenuation of the AF. In this paper, we assume that the channel matrix $\mathbf{H}$ is accurately acquired at the receiver; this is done with the aid of pilot symbols that are periodically inserted in the transmitted symbols.

B. Decoding Complexity

Importantly, in our VLC-MIMO scheme, the AF is designed such that the channel matrix $\mathbf{H}$ is nearly diagonal and full rank. This can be achieved by eliminating the ICI paths and allowing only element-by-element desirable paths. Hence, at the receiver, the transmitted symbols are estimated from the received signals $\mathbf{y}$, the estimated channel matrix $\mathbf{H}$, and the noise variance σ^2; there is no need for complicated detection algorithms, unlike with the classic RF spatial-multiplexing MIMO systems [5]. This is one of the explicit benefits of the proposed scheme.

We also note that the signal search space required for the conventional spatial-multiplexing MIMO receiver per symbol duration is as high as L^{N_t}, which exponentially increases with the number of transmit LEDs. Although the high decoding complexity associated with the conventional spatial-multiplexing VLC-MIMO receiver may be reduced with the aid of suboptimal detection algorithms [5], it still imposes a high burden, especially for high-rate scenarios. In contrast, due to the narrow-window AF, the proposed ICI-free element-by-element VLC-MIMO does not rely on spatial multiplexing, and hence there is a substantial reduction in the decoding complexity: from L^{N_t} to $N_t L$.

C. Channel Capacity and Illustrative Example

In this paper, we evaluate the achievable performance of the VLC-MIMO scheme in terms of the instantaneous channel capacity; we do this in a way similar to that used in previous studies [10], [17], [35]. This is because, with the aid of powerful channel-coding schemes, near-capacity performance can be attained in practice, such as in low-density parity-check and turbo codes [36], [37]. The instantaneous unconstrained channel capacity is given by [10]

$$C = \log_2 \left[\det \left(\mathbf{I}_{N_r} + \frac{P}{\sigma^2 N_t B_{\mathrm{W}}} \mathbf{H}\mathbf{H}^T \right) \right], \tag{4}$$

where $\mathbf{I}_{N_r}$ represents the identity matrix of size N_r, P is the transmit power of each LED (assumed to be the same for all), and B_{W} is the bandwidth. Note that in the previous VLC-MIMO studies, the BER has typically been used as the metric for evaluating reliability, and it has been assumed that the channel-uncoded VLC-MIMO system uses a particular modulation scheme. This has been done because the channel model of an indoor VLC system is deterministic rather than stochastic, and hence, a statistical evaluation of the ergodic channel capacity is unavailable. The same limitations hold true for our analysis, which uses the instantaneous unconstrained channel capacity given in (5). However, the instantaneous unconstrained channel capacity (5) allows us to consider a general upper bound for using a realistic, powerful, near-capacity channel-coding scheme. This implies that, unlike the conventional BER evaluation, our instantaneous capacity analysis is not limited to any specific modulation and channel-encoding schemes.

In order to provide further insight, we consider the scenario in which $N_r = N_t$, that is, the number of transmit LEDs equals the number of receive photodetectors. For the LOS environment considered here, in the conventional VLC-MIMO scheme without a narrow-window AF, all the coefficients in the channel matrix $\mathbf{H}$ tend to have similar values. This typically causes the channel matrix to be low rank, and hence the channel capacity (5) becomes low, which implies the absence of a multiplexing gain. In order to combat this limitation, there needs to be sufficiently wide spacing of the elements both at the transmitter and at the receiver [6].

In contrast to the conventional VCL-MIMO system, in the proposed architecture, the channel matrix is maintained to be nearly diagonal, i.e., $\mathbf{H} = \mathrm{diag}[h_{11}, \cdots, h_{N_r N_r}]$, where diag[•] is the diagonal operation. Therefore, the channel capacity is approximated by

$$C = \sum_{i=1}^{N_r} \log_2 \left(1 + \frac{P}{\sigma^2 N_t B_w} h_{ii}^2 \right), \tag{5}$$

implying that the capacity is the sum of the parallel substreams.

III. Angular Filter

In our proposed architecture for an element-by-element MIMO, shown in Fig. 1, it is desirable for the AF to have a transmission of unity in the angular window of width $2\psi_d$ and zero transmission at all other angles; in the ideal case, this is characterized mathematically by using a step function for the transmission coefficient. From the engineering viewpoint, the deviation from the ideal case needs to be carefully investigated. In particularly, in our MIMO system, any insertion loss in the angular transmission window would degrade the SNR, and a gradual change from transmission to suppression would result in other transmit LEDs, which would result in ICI at the receive photodetectors. Therefore, we investigate the insertion loss (in particular, ripples) in the transmission window, and the steepness of the slope from transmission to suppression in an AF. We present a brief overview of the design of the AF [34], and then we determine the filter response that is suitable for our MIMO system.

Fig. 2 shows the configuration of the AF. The AF consists of an alternating stack of films mate of two different materials. Here, we assume these materials are TiO_2 and SiO_2, which have refractive indices of $n_T = 2.4$ and $n_S = 1.45$, respectively. These films are numbered from $j = 1$ to l, where l is the total number of layers. This structure can be regarded as a host PC ($j = m$ to $l - m + 1$) that has two antireflection PCs ($j = 1$ to m and $j = l - m + 1$ to l). For s-polarization, the electric field is normal to the incident plane, and for p-polarization, the magnetic field is normal to that plane. Note that the modulation bandwidth of the VLC system is typically much narrower than the transmit LED bandwidth. Hence, the target AF characteristics only have

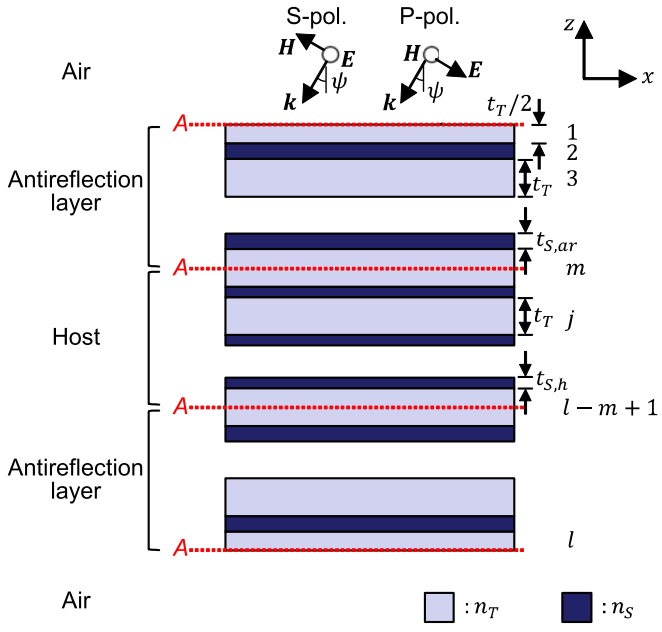

Fig. 2. Configuration of an AF consisting of a one-dimensional photonic crystal; $n_T = 2.4$, $n_S = 1.45$, $t_T = 224$ nm, $t_{S,h} = 96$ nm, $t_{S,ar} = 99$ nm, $l = 109$, $m = 15$.

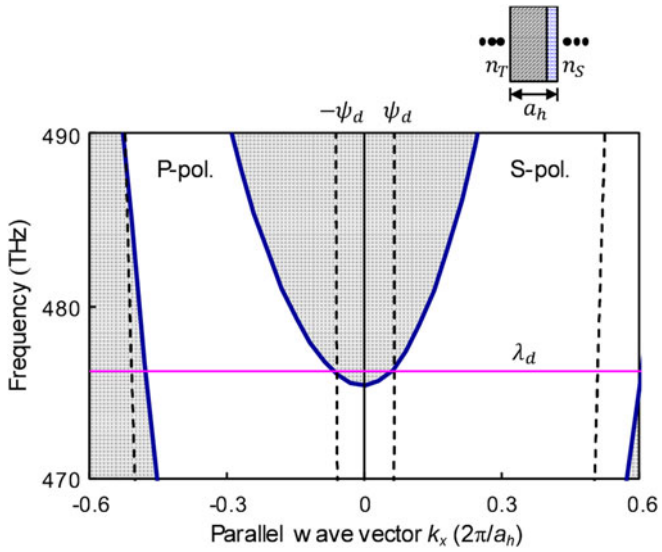

Fig. 3. Dispersion diagram of the host PC. The design angle is $2\psi_d$=14°, and the design wavelength is $\lambda_d = 630$ nm. The design angle and the light line are respectively indicated by the inner and outer oblique black dashed lines.

to be satisfied in a specific carrier frequency with a narrow bandwidth.

In the structure shown in Fig. 2, the angular width of the transmission window is determined by the host PC. Fig. 3 shows the dispersion diagram of the host PC; this is obtained by the plane-wave expansion method [38]. Here, we set the design angle to $2\psi_d = 14°$ (inner oblique black dashed lines) at the design wavelength of $\lambda_d = 630$ nm (horizontal pink solid line). The thicknesses of $t_T = 224$ nm for the TiO_2 films and $t_{S,h} = 96$ nm for the SiO_2 films in the host PC were selected so

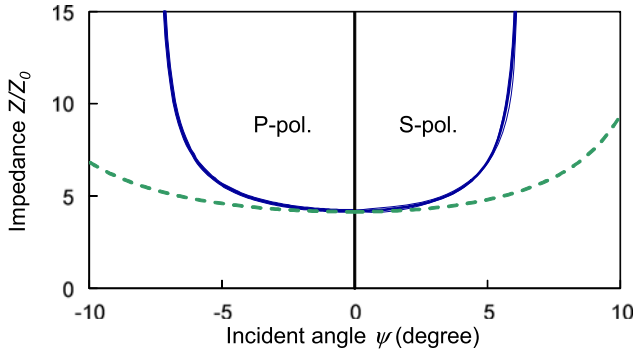

Fig. 4. Angular dependency of the transverse impedance Z_h in the host PC (blue solid line) at the center of the TiO_2 layer. The green dashed line represents Z_{ar}^2/Z_{air}, which comes from the antireflection condition. The transverse impedance is normalized with respect to the free-space impedance Z_0.

that the region in which propagation is allowed (shaded area) is within the transmission angular window ($2\psi_d$ at λ_d), and there is a bandgap (i.e., region in which propagation is inhibited) at all other angles; here, the light lines (outer oblique black dashed lines) correspond to the angle of 90°. Note that for large angles ($\psi > 70°$) of p-polarization, there is a region in which propagation is allowed and the light leaks out; this will be discussed below.

Such a narrow angular window requires the operation of a host PC near the band edge in the dispersion diagram, as shown in Fig. 3, and thus a large impedance mismatch will occur at the interface of the host PC and the air structure. An antireflection PC, in which the thickness is $t_T = 224$ nm for the TiO_2 films and $t_{S,ar} = 99$ nm for the SiO_2 films, enables the reflection to be sufficiently suppressed, resulting in a highly efficient angular transmission response. The antireflection PC is designed as follows. It is well known that the wave impedance of PCs is dependent on local observation points. Thus, the wave impedance, in general, has complex values. The key observation from Fig. 2 is that for the host PC, the antireflection PC, and the air structure, the transverse impedance can be made to take a real value at each interface (denoted by A) if we appropriately select the center of films; here we let the first layer $j = 1$ and the last layer $j = l$ have the same half thickness, $t_T/2$. By ensuring that the transverse impedances have real values at the interfaces, we can design the antireflection structure by using a general impedance-matching methodology.

Fig. 4 shows the angular dependency of the impedance Z_h (blue solid line) of the host PC and compares it with Z_{ar}^2/Z_{air} (green dashed line), where $Z_{air} = Z_0/\cos\psi$ for s-polarization and $Z_{air} = Z_0 \cos\psi$ for p-polarization. Also, Z_0 is the free space impedance, and Z_{ar} is the impedance of the antireflection PC. We see that $Z_{air} Z_h \sim Z_{ar}^2$ is satisfied within ψ_d. In addition, the antireflection PC has $m = 15$ layers, and thus its length is equivalent to that of a quarter of a guided wavelength. Therefore, the antireflection condition is satisfied, and the reflection at the PC-air interference can be sufficiently suppressed.

For the AF shown in Fig. 2, we used the transfer matrix method [39] to calculate the transmission coefficient, which is

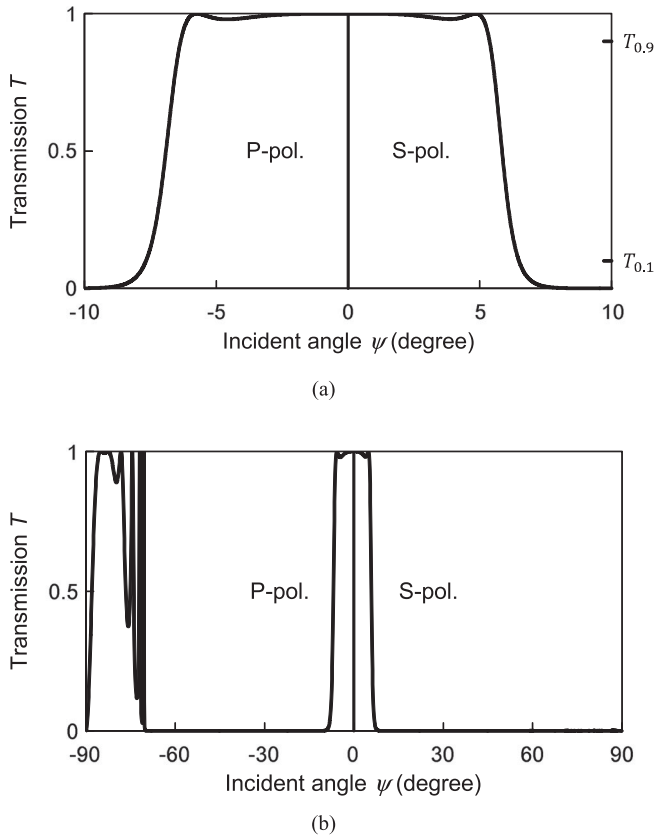

Fig. 5. For the filter shown in Fig. 2, angular response for s-polarization (right panel) and p-polarization (left panel) when the number of layers is $l = 109$. Angular ranges: (a) -10° to 10°, and (b) -90° to 90°.

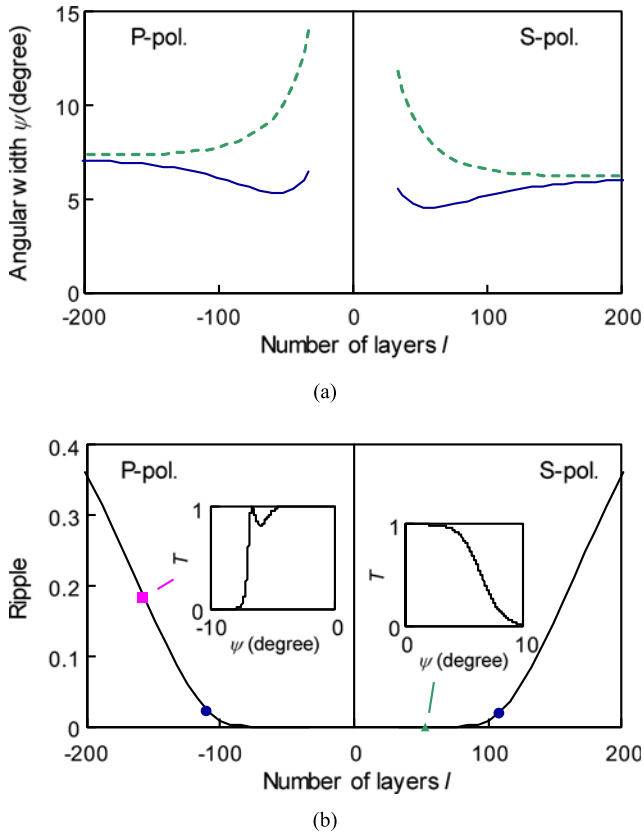

Fig. 6. Variation in the angular widths as a function of the number of layers l, where the number of layers ($m = 15$) in the antireflection PC is fixed. Angular widths for transmission coefficients of $T_{0.9} = 0.9$ and $T_{0.1} = 0.1$ (see Fig. 5(a)) are indicated by the blue solid line and green dashed line, respectively. (b) Ripples in the transmission window for various values of N. The insets show typical angular responses when $N = 53$ for s-polarization (green triangle) and when $N = 157$ for p-polarization (pink square). The blue circles indicate where $N = 109$ (Fig. 5).

plotted in Fig. 5(a) for an angular range of 0 to 10° and in Fig. 5(b) for the full range of s-polarization and p-polarization. We assume the lossless model in which $T + R = 1$, where T and R are the power transmission and reflection coefficients of the entire structure shown in Fig. 2. We see that the desired transmission window is obtained for both polarizations; the half-power angular width $2\psi_d$ is 11.7° for s-polarization and 13.8° for p-polarization. Note that in p-polarization, light transmission occurs for large angles ($\psi > 70^\circ$). In our MIMO system, direct light paths between transmitting and receiving elements have a higher SNR than do indirect light paths, and thus, when evaluating the communication performance in Section IV, we will ignore the effect of indirect light from large incident angles.

In the high-transmission filter of Fig. 2, the number of layers in the host PC can be varied, but the number of layers in the antireflection PCs needs to be fixed at $m = 15$. In other words, we have a design parameter for layer number l for determining the filter response. Figures 6(a) and 6(b) show the variation in the angular width and ripples, respectively, with respect to the number of layers. In Fig. 6(a), angular widths at transmission powers of 0.9 and 0.1 are represented by the blue solid line and the green dashed line, respectively. Frequency responses for $N = 53$ for s-polarization and $N = 157$ for p-polarization, which are typical examples, are presented in the insets of Fig. 6(b). As the number of layers increases, there is a steep angular transition from transmission to suppression, that is, the small difference between the blue solid line and the green dashed line in Fig. 6(a), and ripples occur in the transmission window (Fig. 6(b)). Thus, there exists an optimum range for the number of layers; we selected a value in this range ($l = 109$) for our MIMO system. The current nanofabrication technology for multilayers of wavelength and polarization filters [30], [31] can be used for our structure.

IV. Performance Evaluation

In this section, we evaluate the performance of our proposed AF-aided element-by-element VLC-MIMO system. The parameters used in our simulations are listed in Table I. The array type of the transmitter and the receiver was square, where the numbers of elements at the transmitter and the receiver were set to $N_t = N_r = 4 \times 4 = 16$. The modulation bandwidth was 40 MHz. The height of the room was 1.75 m, and the transmitter semiangle and the photodetector FOV were $\Phi/2 = \Psi/2 = 60^\circ$. The photodetector area was 1×10^{-6} m^2, and the photodetector responsivity was 1 A/W. The element spacings of the transmit LED array and the receive photodetector array were

TABLE I
PARAMETERS USED IN THE SIMULATIONS

Type of transmit and receive arrays	Square array
Number of transmit LEDs	16 (4×4)
Number of receive photodetectors	16 (4×4)
Channels	LOS
Bandwidth	40 MHz
Height H	1.75 m
Transmitter semiangle $\Phi/2$	60°
Field-of-view of photodetectors $\Psi/2$	60°
Photodetector area A	1×10^{-6} m^2
Photodetector responsivity	1 A/W
Spacing between LEDs d_1	0.1 m
Spacing between photodetectors d_2	0.1 m
Noise current density of transimpedance amplifier	5 pA/$\sqrt{\text{Hz}}$

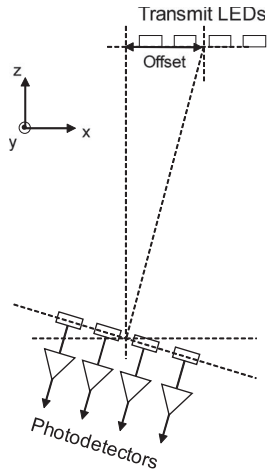

Fig. 7. Offset model considered in our simulations; the transmitter has an offset in the x direction, and the receiver is directed toward the transmitter.

set to $d_1 = d_2 = 0.1$ m, and the noise current density of the transimpedance amplifier was 5 pA/$\sqrt{\text{Hz}}$.

The offset model considered in our simulations is shown in Fig. 7; the transmitter has an offset Δ in the x direction, and the receiver is directed toward the transmitter.

Before performing simulations with the specific photonic-crystal-based AF designed in Section III, we evaluated the fundamental characteristics of our AF-aided element-by-element VLC-MIMO system. We considered the use of an ideal step-function AF with a threshold angle ψ_0. The angular response is

$$r(\psi) = \begin{cases} 1 & (\psi \le \psi_0) \\ 0 & (\psi > \psi_0) \end{cases}. \tag{6}$$

Fig. 8 shows the unconstrained instantaneous capacity of this scheme for threshold angles of $\psi_0 = 1°$, 7°, 10°, 20°, and 60°. The capacity bound (5) of the ICI-free approximation is also shown. For simplicity, the offset Δ was set to zero. The scenario of $\psi_0 = 60°$ corresponds to the conventional VLC-MIMO system, which does not rely on the AF, since here, the FOV of the photodetectors was set to $\psi_0 = 60°$. Observe in Fig. 8 that when $\psi_0 = 1°$, 7°, and 10°, the proposed AF-aided MIMO schemes performed better than the conventional AF-aided VLC-MIMO

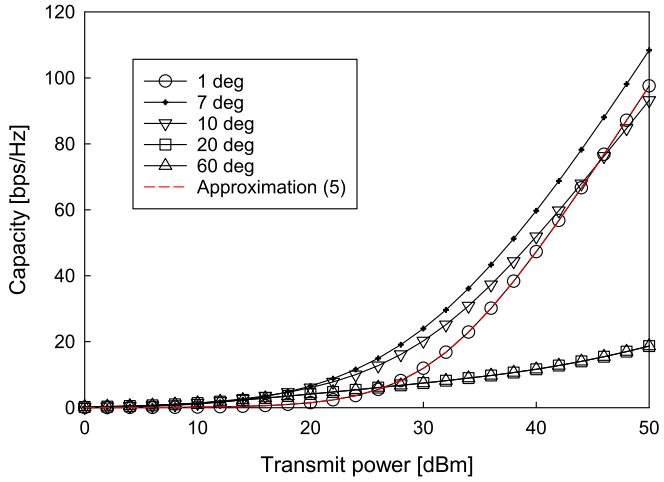

Fig. 8. Capacity comparisons of the proposed AF-aided MIMO scheme using the ideal step-function AF, for threshold angles of $\psi_0 = 1°$, 7°, 10°, 20°, and 60°. The ICI-free capacity approximation of (5) is also shown.

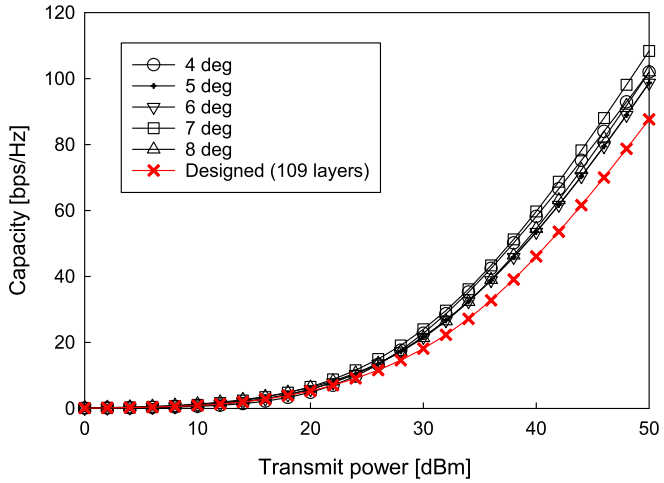

Fig. 9. Capacity comparisons of the proposed AF-aided MIMO scheme using a filter with a window of 15°, and the ideal step-function AFs for threshold angles of $\psi_0 = 4°$, 5°, 6°, 7°, and 8°.

scheme, while when $\psi_0 = 20°$, it did not. The best performance was obtained by the proposed scheme with $\psi_0 = 7°$, although the proposed scheme with $\psi_0 = 1°$ corresponds to the ICI-free scenario, which is the analytical ICI-free approximation of (5). This implies that a reduced interference factor increases the capacity, especially in the low-SNR regime.

In Fig. 9, we show the unconstrained instantaneous capacity of the proposed AF-aided MIMO scheme using the specific AF of Fig. 5, with a window of approximately $2\psi_d = 13°$. The associated capacity curves of the ideal step-function AFs are also shown for threshold angles of $\psi_0 = 4°$, 5°, 6°, 7°, and 8°.

In Fig. 9, it can be seen that our proposed VLC-MIMO with an AF achieved the expected gain; this was due to the multiple decoupled parallel streams and the small performance loss from the ideal-filter counterpart. This occurs because the angular transmission response of the AF is expressed by the averaged

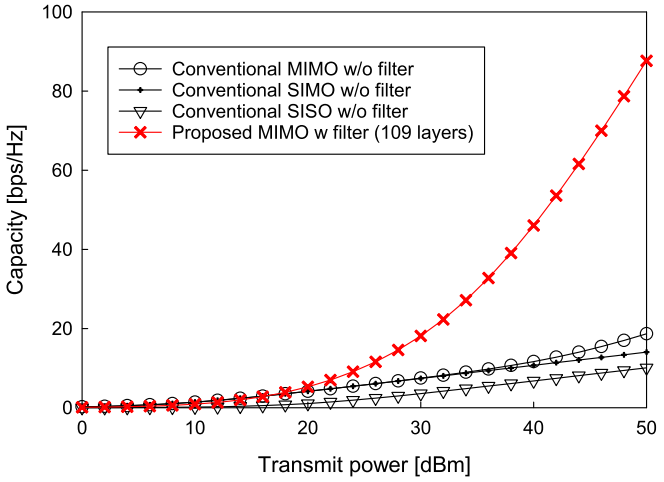

Fig. 10. Capacity comparisons between the proposed AF-aided MIMO scheme and the conventional MIMO arrangements; both systems used a 4×4 array at both the transmitter and the receiver.

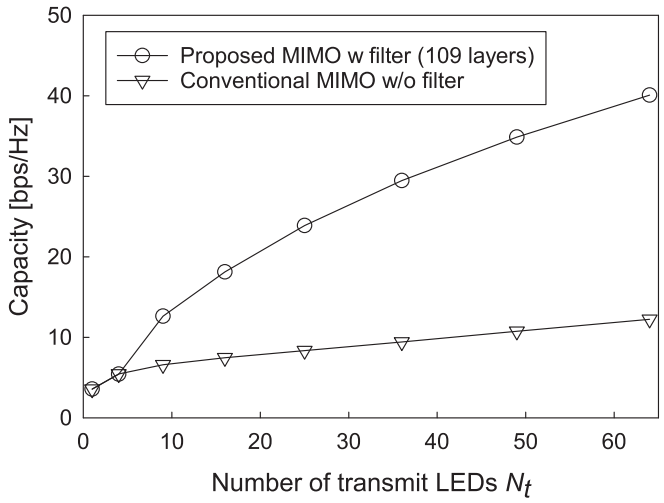

Fig. 11. Unconstrained instantaneous capacity of our proposed scheme and that of the conventional MIMO scheme (without an AF). The number of transmit LEDs varied from $N_t = 1$ to 64, with the same number of receive photodetectors. The total transmit power was 30 dBm.

response of the p-polarization and the s-polarization. Note that the resultant effective angular transmission response of the AF designed in Fig. 5 was not as steep as that of the ideal step-function AF.

Fig. 10 shows the unconstrained instantaneous capacity of our proposed system. The benchmark schemes were the conventional spatial-multiplexing VLC-MIMO scheme, which does not rely on an AF at the receiver, a single-input single-output (SISO) scheme, and a single-input multiple-output (SIMO) scheme. Observe that in Fig. 10, our proposed scheme achieved the highest capacity, and the difference between it and the other benchmark schemes increased as the transmit power increased. This occurred primarily because the proposed scheme was able to exploit the multiplex gain in an effective manner, but none of the benchmark schemes were able to do so. Note that in the low SNR region, the proposed VLC-MIMO scheme was slightly outperformed by the conventional VLC-MIMO scheme, although it was not substantially high. This is because the total receive power, rather than the channel rank, plays an important role in the low SNRs. However, the explicit benefit of the proposed scheme remained unchanged, since we focused our attention on the high-SNR scenario, similar to the conventional indoor-VLC studies [4], [7], [40].

Next, we evaluated the rate scalability of the proposed scheme with respect to the number of transmit LEDs and the number of receive photodetectors; the results are shown in Fig. 11. We varied the number of transmit LEDs from $N_t = 1$ to 64, with the same number of receive photodetectors. The total transmit power was 30 dBm, and the other system parameters remained unchanged. It can be seen in Fig. 11 that when $N_t \geq 9$, our proposed scheme performed better than did the conventional method, and the difference increased as the number of transmit LEDs increased. This occurred due to the effective decoupling of the parallel symbol streams at the receiver.

Finally, we investigated the effects of the alignment offset Δ between the transmitter and the receiver, as shown in Fig. 7.

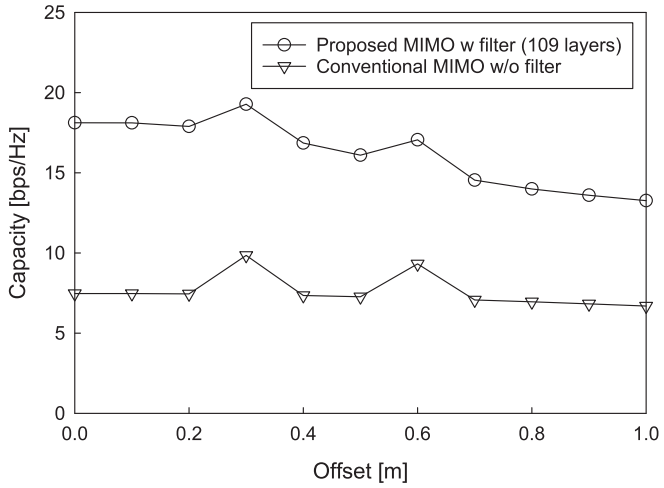

Fig. 12. Unconstrained instantaneous capacity of our proposed scheme (with AF) and the conventional MIMO scheme (without AF). The transmit power was 30 dBm.

In Fig. 12, we show the unconstrained instantaneous capacity of our proposed scheme (with AF) and that of the conventional MIMO scheme (without AF). The offset was varied from $\Delta = 0$ to 1.0 m, and the total transmit power was 30 dBm. Observe in Fig. 12 that the alignment offset between the receiver and the transmitter did not result in any significant loss of performance, and the capacity was higher than that of the conventional MIMO scheme, as expected. We assumed that the receiver unit was aligned to the transmitter in the simulations of Fig. 12. The same assumption may be made in the conventional imaging and non-imaging VLC receivers [1], [3], [14], [41]. In order to satisfy this requirement, the mechanical scan of [42] is readily applicable to our VLC-MIMO receiver, which is achieved at the sacrifice of additional cost and complexity.

V. Conclusions

In this paper, we have proposed a novel AF-aided element-by-element VLC-MIMO system that allows parallel transmission and reception of symbol streams in a practical LOS-channel scenario. In order to configure the narrow-window AF structure, we employed a one-dimensional photonic crystal; the design guidelines are provided herein. Our proposed scheme is a low-complexity symbol-by-symbol detection scheme, regardless of the number of parallel symbol streams. Our simulation results demonstrated that our proposed scheme performs better than do the conventional VLC-MIMO schemes, and the advantage increases with the number of transmit LEDs.

References

[1] T. Komine and M. Nakagawa, "Fundamental analysis for visible-light communication system using LED lights," *IEEE Trans. Consum. Electron.*, vol. 50, no. 1, pp. 100–107, Feb. 2004.

[2] S. Hranilovic, *Wireless Optical Communication Systems*. New York, NY, USA: Springer, 2005.

[3] H. Elgala, R. Mesleh, and H. Haas, "Indoor optical wireless communication: Potential and state-of-the-art," *IEEE Commun. Mag.*, vol. 49, no. 9, pp. 56–62, Sep. 2011.

[4] L. Hanzo, H. Haas, S. Imre, D. O'Brien, M. Rupp, and L. Gyongyosi, "Wireless myths, realities, and futures: From 3G/4G to optical and quantum wireless," *Proc. IEEE*, vol. 100, no. Special Centennial Issue, pp. 1853–1888, May 2012.

[5] S. Sugiura, S. Chen, and L. Hanzo, "MIMO-aided near-capacity turbo transceivers: Taxonomy and performance versus complexity," *IEEE Commun. Surveys Tut.*, vol. 14, no. 2, pp. 421–442, May 2012.

[6] D. Takase and T. Ohtsuki, "Spatial multiplexing in optical wireless MIMO communications over indoor environment," *IEICE Trans. Commun.*, vol. 89, no. 4, pp. 1364–1371, 2006.

[7] L. Zeng *et al.*, "High data rate multiple input multiple output (MIMO) optical wireless communications using white LED lighting," *IEEE J. Sel. Areas Commun.*, vol. 27, no. 9, pp. 1654–1662, Dec. 2009.

[8] K. D. Dambul, D. C. O'Brien, and G. Faulkner, "Indoor optical wireless MIMO system with an imaging receiver," *IEEE Photon. Technol. Lett.*, vol. 23, no. 2, pp. 97–99, Jan. 2011.

[9] A. H. Azhar, T. Tran, and D. O'Brien, "A gigabit/s indoor wireless transmission using MIMO-OFDM visible-light communications," *IEEE Photon. Technol. Lett.*, vol. 25, no. 2, pp. 171–174, Jan. 2013.

[10] P. M. Butala, H. Elgala, and T. D. C. Little, "SVD-VLC: A novel capacity maximizing VLC MIMO system architecture under illumination constraints," in *Proc. IEEE Global Telecommun. Conf. Workshops*, Atlanta, GA, USA, Dec. 2013, pp. 1087–1092.

[11] Y. Wang and N. Chi, "Demonstration of high-speed 2×2 non-imaging MIMO Nyquist single carrier visible light communication with frequency domain equalization," *J. Lightw. Technol.*, vol. 32, no. 11, pp. 2087–2093, Jun. 2014.

[12] S. Sugiura, S. Chen, and L. Hanzo, "A universal space-time architecture for multiple-antenna aided systems," *IEEE Commun. Surveys Tut.*, vol. 14, no. 2, pp. 401–420, May 2012.

[13] M. Di Renzo, H. Haas, A. Ghrayeb, S. Sugiura, and L. Hanzo, "Spatial modulation for generalized MIMO: Challenges, opportunities and implementation," *Proc. IEEE*, vol. 102, no. 1, pp. 1–47, Jan. 2014.

[14] R. Mesleh, H. Elgala, and H. Haas, "Optical spatial modulation," *IEEE/OSA J. Opt. Commun. Netw.*, vol. 3, no. 3, pp. 234–244, Mar. 2011.

[15] W. O. Popoola, E. Poves, and H. Haas, "Error performance of generalised space shift keying for indoor visible light communications," *IEEE Trans. Commun.*, vol. 61, no. 5, pp. 1968–1976, May 2013.

[16] W. O. Popoola and H. Haas, "Demonstration of the merit and limitation of generalised space shift keying for indoor visible light communications," *J. Lightw. Technol.*, vol. 32, no. 10, pp. 1960–1965, May 2014.

[17] N. Ishikawa and S. Sugiura, "Maximizing constrained capacity of power-imbalanced optical wireless MIMO communications using spatial modulation," *J. Lightw. Technol.*, vol. 33, no. 2, pp. 519–527, Feb. 2015.

[18] E. Bayaki and R. Schober, "On space-time coding for free-space optical systems," *IEEE Trans. Commun.*, vol. 58, no. 1, pp. 58–62, Jan. 2010.

[19] T. Q. Wang, Y. A. Sekercioglu, and J. Armstrong, "Analysis of an optical wireless receiver using a hemispherical lens with application in MIMO visible light communications," *J. Lightw. Technol.*, vol. 31, no. 11, pp. 1744–1754, Jun. 2013.

[20] Y. Alqudah and M. Kavehrad, "MIMO characterization of indoor wireless optical link using a diffuse-transmission configuration," *IEEE Trans. Commun.*, vol. 51, no. 9, pp. 1554–1560, Sep. 2003.

[21] T. Fath and H. Haas, "Performance comparison of MIMO techniques for optical wireless communications in indoor environments," *IEEE Trans. Commun.*, vol. 61, no. 2, pp. 733–742, Feb. 2013.

[22] T. Q. Wang and J. Armstrong, "Performance of indoor MIMO optical wireless system using linear receiver with prism array," in *Proc. 2014 Aust. Commun. Theory Workshop*, Feb. 2014, pp. 51–56.

[23] T. Q. Wang, C. He, and J. Armstrong, "Angular diversity for indoor MIMO optical wireless communications," in *Proc. IEEE Int. Conf. Commun.*, 2015, pp. 5066–5071.

[24] T. Q. Wang, R. J. Green, and J. Armstrong, "MIMO optical wireless communications using ACO-OFDM and a prism-array receiver," *IEEE J. Sel. Areas Commun.*, vol. 33, no. 9, pp. 1959–1971, Sep. 2015.

[25] C. He, T. Q. Wang, and J. Armstrong, "Performance of optical receivers using photodetectors with different fields of view in a MIMO ACO-OFDM system," *J. Lightw. Technol.*, vol. 33, no. 23, pp. 4957–4967, Dec. 2015.

[26] J. D. Joannopoulos, S. G. Johnson, J. N. Winn, and R. D. Meade, *Photonic Crystals: Molding the Flow of Light*. Princeton, NJ, USA: Princeton Univ. Press, 2011.

[27] H. A. Macleod, *Thin-Film Optical Filters*. Boca Raton, FL, USA: CRC Press, 2001.

[28] Y. Fink *et al.*, "A dielectric omnidirectional reflector," *Science*, vol. 282, no. 5394, pp. 1679–1682, 1998.

[29] L. Maigyte and K. Staliunas, "Spatial filtering with photonic crystals," *Appl. Phys. Rev.*, vol. 2, no. 1, 2015, Art. no. 011102.

[30] Y. Shen, C. W. Hsu, Y. X. Yeng, J. D. Joannopoulos, and M. Soljačić, "Broadband angular selectivity of light at the nanoscale: Progress, applications, and outlook," *Appl. Phys. Rev.*, vol. 3, no. 1, 2016, Art. no. 011103.

[31] Y. Shen, D. Ye, I. Celanovic, S. G. Johnson, J. D. Joannopoulos, and M. Soljačić, "Optical broadband angular selectivity," *Science*, vol. 343, no. 6178, pp. 1499–1501, 2014.

[32] R. E. Hamam, I. Celanovic, and M. Soljačić, "Angular photonic band gap," *Physical Rev. A*, vol. 83, no. 3, 2011, Art. no. 035806.

[33] Y. Shen *et al.*, "Metamaterial broadband angular selectivity," *Physical Rev. B*, vol. 90, no. 12, 2014, Art. no. 125422.

[34] H. Iizuka, N. Engheta, and S. Sugiura, "Extremely small wavevector regime in a one-dimensional photonic crystal heterostructure for angular transmission filtering," *Opt. Lett.*, vol. 41, no. 16, pp. 3829–3832, Aug. 2016.

[35] N. Ishikawa and S. Sugiura, "EXIT-chart-based design of irregular precoded power-imbalanced optical spatial modulation," in *Proc. IEEE Veh. Technol. Conf.*, Boston, MA, USA, Sep. 2015, pp. 1–5.

[36] W. E. Ryan and S. Lin, *Channel Codes: Classical and Modern*. Cambridge, U.K.: Cambridge Univ. Press, 2009.

[37] L. Hanzo, T. Liew, B. Yeap, R. Y. S. Tee, and S. X. Ng, *Turbo Coding, Turbo Equalisation, and Space-Time Coding for Transmission Over Fading Channels*. Hoboken, NJ, USA: Wiley, 2011.

[38] K. Ho, C. T. Chan, and C. M. Soukoulis, "Existence of a photonic gap in periodic dielectric structures," *Physical Rev. Lett.*, vol. 65, no. 25, pp. 3152–3155, 1990.

[39] B. E. A. Saleh and M. C. Teich, *Fundamentals of Photonics*, 2nd ed. Hoboken, NJ, USA: Wiley, 2007.

[40] J. Grubor, S. Randel, K.-D. Langer, and J. W. Walewski, "Broadband information broadcasting using LED-based interior lighting," *J. Lightw. Technol.*, vol. 26, no. 24, pp. 3883–3892, Dec. 2008.

[41] Z. Ghassemlooy, W. Popoola, and S. Rajbhandari, *Optical Wireless Communications: System and Channel Modelling with MATLAB*. Boca Raton, FL, USA: CRC Press, 2012.

[42] M. Nakagawa *et al.*, "Illuminative light communication device," U.S. Patent 7 583 901 B2, Sep. 1, 2009. [Online]. Available: https://www.google.com/patents/US7583901

Shinya Sugiura (M'06–SM'12) received the B.S. and M.S. degrees in aeronautics and astronautics from Kyoto University, Kyoto, Japan, in 2002 and 2004, respectively, and the Ph.D. degree in electronics and electrical engineering from the University of Southampton, Southampton, U.K., in 2010.

From 2004 to 2012, he was a Research Scientist with the Toyota Central Research and Development Laboratories, Inc., Nagakute, Japan. Since 2013, he has been an Associate Professor with the Department of Computer and Information Sciences, Tokyo University of Agriculture and Technology, Tokyo, Japan, where he is the Head of the Wireless Communications Research Group. He authored or coauthored more than 70 refereed research publications, including 45 IEEE journals and magazine papers. His research interests include wireless communications, networking, signal processing, and antenna technology.

Dr. Sugiura received a number of awards, including the Young Scientists' Prize by the Minister of Education, Culture, Sports, Science, and Technology of Japan in 2016, the 14th Funai Information Technology Award (First Prize) from the Funai Foundation in 2015, the 28th Telecom System Technology Award from the Telecommunications Advancement Foundation in 2013, the sixth IEEE Communications Society Asia-Pacific Outstanding Young Researcher Award in 2011, the 13th Ericsson Young Scientist Award in 2011, and the 2008 IEEE Antennas and Propagation Society Japan Chapter Young Engineer Award. He was also certified as an Exemplary Reviewer of the IEEE COMMUNICATIONS LETTERS in 2013 and 2014.

Hideo Iizuka (M'04) received the B.S. and M.S. degrees in electrical engineering from Saitama University, Saitama, Japan, in 1995 and 1997, respectively, and the Doctorate degree in engineering from the Nagoya Institute of Technology, Nagoya, Japan, in 2007.

In 1997, he joined the Toyota Central Research and Development Laboratories, Inc., Nagakute, Japan. From 2001 to 2002, he was a Visiting Scholar with the University of Birmingham, Birmingham, U.K., and, from 2008 to 2011, with the Toyota Research Institute, Toyota Motor Engineering and Manufacturing North America, Inc., Ann Arbor, MI, USA. His current research focuses on the analysis and the development of electromagnetic devices and systems for automotive applications.

Dr. Iizuka received the IEICE Young Engineering Award in 2001.